Tellus (1980) *32*, 326–339

An application of a simple diagnostic cloud model to the 20 May 1977 storms over the Oklahoma meso-network

By SOON-UNG PARK and DHIRENDRA N. SIKDAR, *Atmospheric Sciences, University of Wisconsin-Milwaukee, Milwaukee, Wisconsin 53201, U.S.A.*

(Manuscript received June 8, 1979; in final form January 16, 1980)

ABSTRACT

The average mesoscale environmental properties such as mass, moisture and vorticity that produce heavy rain have been computed by kinematic techniques for the 20 May 1977 severe storm using NSSL meso-network observations. A simple steady-state cloud model derived from the conservation law is applied to these storm data. The rainfall estimated by the condensation rate of the cloud model agrees fairly well with that observed at the ground. The total energy of the storm system is largely supported by the latent heat release.

1. Introduction

In recent years the interaction of cumulus clouds with larger scales of motion has attracted lively interest in the meteorological community. Most attention has been given to the interaction between tropical cumulus convection and synoptic-scale forcing (Yanai et al. 1973; Arakawa and Schubert, 1974; Ogura and Cho, 1973, etc.). The basic underlying physics of this interaction is manifested by subsidence induced through mass conservation, mixing of cloud and environmental properties, subcloud evaporation, and precipitation.

In the mid-latitudes, the organization of intense convection into mesoscale systems often causes devastating flash floods or wind damage, but the interactions between mesoscale systems and thunderstorm activities are still mainly unexplored. One of the reasons for this neglect is that the conventional observational networks are too sparse to resolve the mesoscale systems satisfactorily. The interaction mechanism itself is also quite involved; for instance, the first clouds, which are initiated by convection due to the release of potential instability, are restrained as they build into the dry layer above by evaporative cooling of the entrained air. The environment near the cloud will be cooled as the cloud evaporates, so a more favorable cloud-developing environment will be formed through reduction of the stable stratification. Subsequent clouds will then continue to build into this less stable, more moist area. The net latent heat released as a result of precipitation will heat the area, thereby enhancing convection through increased lifting and low-level moisture convergence.

The purpose of this study is to investigate the modification of the mesoscale environment due to cumulus convection, through parameterization of the preassigned mass distribution function (or entrainment rate) and making use of conservation quantities. For this purpose we have chosen the 20 May 1977 storm situation, when the Synchronous Meteorological Satellite (SMS) images showed well-organized convective storms over the NSSL meso-network (section 2). These storms produced heavy rainfall, causing flash floods in Oklahoma. The mesoscale budgets such as mass, moisture and vorticity are objectively calculated (section 3) for the storm period over the meso-network. The results are presented in section 4. In order to obtain an estimate for a mass, moisture relationship between the convective cloud system and the associated mesoscale environment, a simple cloud parameterization is described in section 5. This simple cloud model is applied to the storm in section 6.

0040-2826/80-040326-14$02.50/0

2. Synoptic situation

2.1. *Surface development*

In the morning of 20 May 1977, a low-pressure system developed south-east of New Mexico at the end of a stationary front that extended from an occluding cyclonic storm centered in central Canada. At 0900 CST a well-defined meso-low had developed over northern Kansas, accompanied by a well-organized squall line from northern Kansas to south central Oklahoma. At 1500 CST the meso-low merged into the frontal zone that was moving eastward. During the time period from 1500 CST to 1800 CST heavy rain occurred in the NSSL meso-network. Air-mass thunderstorms and showers were occurring far ahead of the front in the broad south-easterly flow from the Gulf of Mexico. (Fig. 1 shows the 1800 CST surface map.)

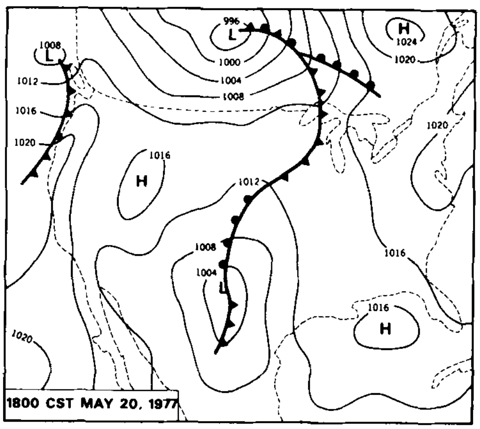

Fig. 1. Surface analysis of synoptic pattern for 1800 CST 20 May 1977.

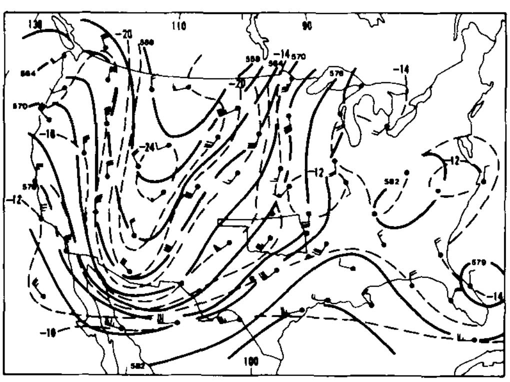

Fig. 2a. 500 mb analysis for 0900 CST. Temperature (– – – –) and geopotential height (————).

2.2 *Upper air features*

These surface disturbances were associated with an upper-level cold trough that moved eastward out of the Rocky Mountains into the Great Plains. The 0900 CST 500-mb analysis (Fig. 2a) shows weak upper-air cold advection in front of the deep trough but rather strong warm advection in the lower troposphere (850–700 mb) over Oklahoma. The low-level southerly jet with maximum wind of 25 m/s lies along a north-east–south-west axis through Oklahoma City at the 850-mb level (Fig. 2b).

2.3. *The precipitation pattern*

The unusual heavy precipitation events over north-western Oklahoma and southern Kansas results in a devastating flash flood in Oklahoma on 20 May 1977. Fig. 3 shows the distribution of the 24-hour rainfall amount obtained from NOAA climate data (1977). The maximum rainfall, more than 100 mm, lies along a west–east axis just north of Oklahoma City, where the 24-hour total rainfall amount recorded on 20 May 1977 was 49 mm.

The maximum rainfall axis lies north of the NSSL meso-network. However, the radar echoes at Oklahoma City in agreement with the satellite images showed the continuous development of convective cells in the southerly wind far south of the network. Some of these cells passed over the network, merged into the major systems lying north of the NSSL network, and caused heavy precipitation in north-western Oklahoma. Newton and

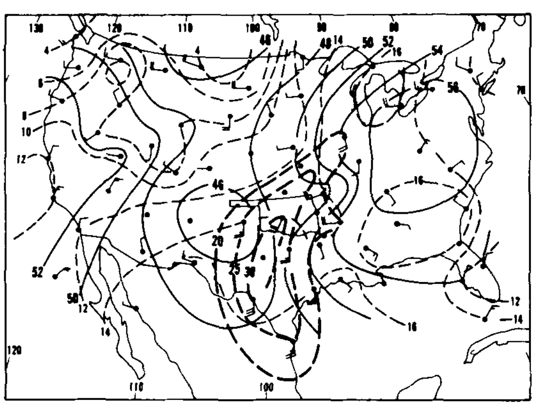

Fig. 2b. 850 mb analysis for 0900 CST indicating low-level southerly jet aligned NE–SW through Oklahoma City. Temperature (– – – –) and geopotential height (————). Bold broken lines are isotachs.

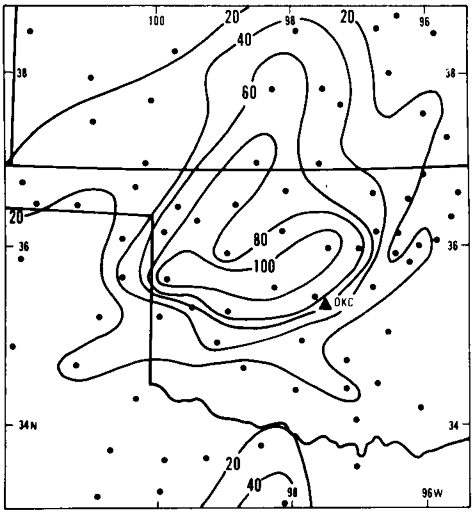

Fig. 3. Rainfall in millimeters during a 24-hour period on 20 May 1977.

Katz (1958) showed that when the wind is veering with height, which is the case in this storm, the maximum relative inflow into the storm occurs on the right flank of the storm, providing for new developments in this region.

Fig. 4 illustrates that, during the period of budget calculation which will be described later, precipitation occurring over the meso-network is due not to the main storm systems to the north but to the convective cells embedded in the moist southerly wind developed to the south-west of Oklahoma City. At 15:15 a small convective cell appeared on the Oklahoma City radar screen and became larger while moving north-eastward (210°) at about 20 m/s, which was roughly 30–40° to the right of, and slightly lower than, the environmental mean wind through the mid-troposphere (not shown here). At 1700 CST it came into the southern part of the meso-network and converged into the main system north of Oklahoma City at about 1725 CST. The maximum precipitation rate in the NSSL meso-network area (Fig. 5) was recorded at this time as high as 98 mm h^{-1}.

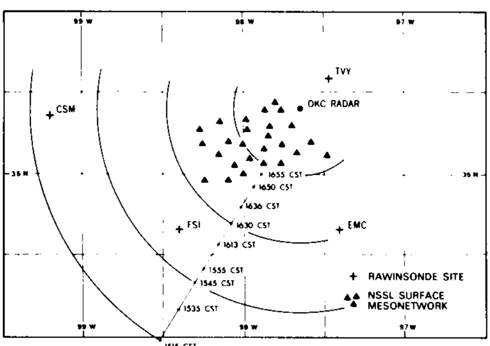

Fig. 4. National Severe Storms Laboratory (NSSL) data area and trace of radar echo which produced heavy rainfall at NSSL meso-network. Dots indicate the locations of the center of radar echoes at various times.

3. Data analysis

The data used in this study include rawinsonde measurements, surface precipitation rates measured in the National Severe Storms Laboratory (NSSL) meso-network, hourly precipitation from NOAA Climate data, and the Oklahoma City radar data, on 20 May 1977.

3.1 *Data reduction*

Rawinsondes were released from four sites (Fig. 4) at approximately 1½–2-hour intervals from 1318 to 2136 CST. During the period of convective activity in the NSSL meso-network area, data were available from all four sites, but not at all four before and after the period of storm activity. Therefore, data analysis was confined to the storm period.

Mesoscale analysis of rawinsonde data should take into account the sonde rise time and down-wind drift (Fankhauser, 1969; McNab and Betts, 1978). The NSSL sondes drifted approximately 55–85 km around 100 mb and reached the 100 mb level 50–70 minutes after launch. Since the data along one sounding path are not valid for a single

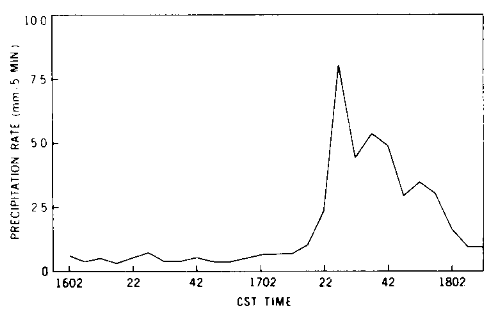

Fig. 5. Observed precipitation rates (5 minutes average) at the NSSL surface meso-network. CST stands for Central Standard Time.

time, because of sonde rise time, a set of successive ascents were used only when at least two of the three successive rawinsondes reached above 100 mb. Two such successive sets of rawinsonde data are needed to make one budget calculation. A total of 44 pressure levels from 965 mb to 105 mb are used for the calculation.

The first step of rawinsonde data reduction is a vertical interpolation of each sounding to evenly spaced pressure levels. A vertical spacing of 20 mb is used to retain the contact point variables using a sample linear regression model such that $Q_i = a_i p + b_i$, where Q_i is the datum obtained from the rawinsondes (i.e. $Q_i = T, u, v, q, \ldots$) and the coefficients a_i, b_i are determined by a least-squares fit of the Q_i's measured at each contact point data. A different set of coefficients is computed for each variable at each vertical data level.

The second step of rawinsonde data reduction is to make a time interpolation of each variable. This has been done using two or three successive sets of sonde data as the linear function of time at each evenly spaced pressure level, also taking into account the sonde rise time, so that we get the desired time soundings.

3.2. *Budget computations*

The choice of the budget area is difficult because of the substantial sonde drift. In this study the budget area is centered over the approximate mid-point of the overlapping data area which is projected downward from the highest level of data points, as in McNab and Betts (1978). Fortunately, this center point falls in the region of the NSSL surface meso-network. The data within this area are approximated as the linear functions of horizontal position: $Q_i = a_i x + b_i y + c_i$. The coefficients, a_i, b_i, c_i are also determined by using a least-squares fit of the Q_i's measured at each balloon position at each level. Two sets of "simultaneous" ascents valid at a common time (1630 and 1800 CST) were obtained from four rawinsonde sites.

Once the horizontal wind components (u, v) at each level are fitted by the linear function of horizontal position of the balloons, the calculations for the dynamic and thermodynamic variables were made. For example, the horizontal divergence $\nabla \cdot \mathbf{v}$, relative vorticity $\bar{\zeta}$, vertical p-velocity $\bar{\omega}$, meso-network apparent heat source Q_1, and apparent moisture sink Q_2, averaged over the overlapping area are evaluated by

$$\overline{\nabla \cdot \mathbf{v}} = \frac{1}{A} \int \int_A \left(\frac{\partial u}{\partial x} + \frac{\partial v}{\partial y} \right) dx dy \tag{1}$$

$$\bar{\zeta} = \frac{1}{A} \int \int_A \left(\frac{\partial v}{\partial x} - \frac{\partial u}{\partial y} \right) dx dy \tag{2}$$

$$\bar{\omega} = \bar{\omega}_0 - \int_{p_s}^{p} \overline{\nabla \cdot \mathbf{v}} \, dp \tag{3}$$

$$Q_1 = \frac{\partial \bar{s}}{\partial t} + \nabla \cdot (\overline{\mathbf{v}s}) + \frac{\partial}{\partial p} (\overline{\omega s}) \tag{4}$$

$$Q_2 = -L \left[\frac{\partial \bar{q}}{\partial t} + \nabla \cdot (\overline{\mathbf{v}q}) + \frac{\partial}{\partial p} (\overline{\omega q}) \right] \tag{5}$$

where A represents the overlapping area, overbars denote area averages, p_s the surface pressure, $\bar{\omega}_0$ the vertical p-velocity at the surface, L the latent heat of condensation, $\bar{q}$ the mixing ratio, and $\bar{s}$ the static energy ($c_p \bar{T} + gz$).

The lower boundary condition of $\bar{\omega}_0$ used at the 965 mb level was estimated from the TVY tower data averaged during the period of 1630 CST to 1800 CST. We assigned tentatively $\bar{\omega}_0 \simeq -0{\cdot}04$ mb/s; the top boundary condition used was $\bar{\omega}_T = 0$ at $p = 105$ mb, which is the top level of data availability. To satisfy these two boundary conditions the original divergence estimates were altered according to O'Brien's (1970) scheme.

4. Mass, heat, moisture and vorticity profiles

Because of rawinsonde data limitation in the time coverage, we analyzed only two time periods of soundings; 1630 and 1800 CST. During this period the NSSL meso-network area was highly disturbed due to the eastward moving main systems north of Oklahoma City and the passage of newly developed convective cells (see Fig. 4) which originated south of the main thunderstorm complex.

Even though budget results indicate significant variations associated with the time variation of the variables, only time mean budgets (from 1630 to 1800 CST) will be considered in the diagnostic cloud modeling, because the soundings used in this study are too few to permit us to examine the time variations accurately.

4.1. *Mean horizontal divergence, relative vorticity and vertical velocity*

Fig. 6 shows the vertical profiles of the horizontal divergence evaluated from eq. (1) over the overlapped area at 1630 to 1800 CST. At 1630 CST, a deep layer of convergence occurred below 350 mb except in the layer between 850–800 mb, where a weak divergence was noticed; strong divergence occurred in the upper layer, around 200 mb. At 1800 CST, the thickness of low-level convergence decreased to 500 mb and upper-level divergence increased both in thickness and amplitude. The low-level weak divergence disappeared at 1800 CST. This might suggest that at 1630 CST the budget area did not lie in the active center but rather than this region was influenced by the near-cloud mid-tropospheric weak subsiding motion. Note that the amplitude of low-level convergence at 1800 CST of magnitude about $-6 \times 10^{-5}\ s^{-1}$ is nearly constant with height. The vertical profiles of divergence are similar to the results obtained by Fankhauser (1974) in the squall line case study, but the values are slightly smaller than his, which was located near the center of the squall line.

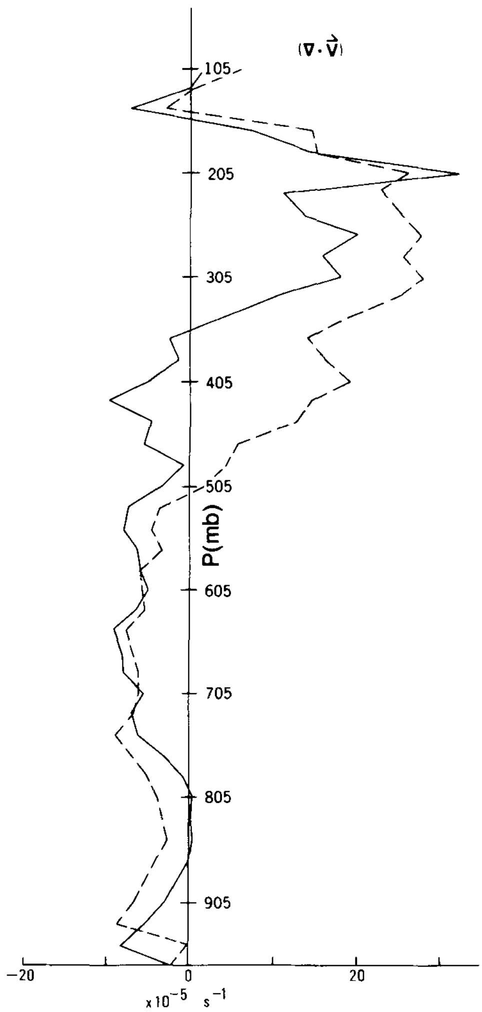

Fig. 6. Adjusted horizontal divergence profiles for 1630 CST (———) and 1800 CST (– – – –).

Fig. 7 illustrates vertical profiles of relative vorticity computed from eq. (2). At 1630 CST the cyclonic circulations are limited to near the surface. There exist deep anticyclonic circulations in the mid-troposphere and upper troposphere, with a maximum near 250 mb. In contrast, at 1800 CST the vertical thickness and amplitude of the cyclonic vorticity in the mid-troposphere increased significantly, especially around 500 mb, while the upper-level anticyclonic vorticity weakened. Anticyclonic vorticity in the lower level is weak and confined to a shallow layer between 860–750 mb.

The vorticity profiles at the two time periods show a similar pattern except for intensification of cyclonic vorticity at 1800 CST. This probably suggests that the budget area was more influenced by active storms later than at 1630 CST. The disturbed condition prevailed even at 1630 CST.

The profiles of the adjusted vertical p-velocity in eq. (3) are illustrated in Fig. 8. Upward motion dominates the whole troposphere at both times. The single maximum value of vertical velocity occurs around 400 mb at 1630 CST and shifts downward to 500 mb at 1800 CST with increased magnitude. The single maximum vertical velocity may imply that deep clouds exist in the budget area during this time period.

4.2. *Apparent heat source, moisture sink and vorticity source*

The time-averaged (90 min.) vertical profile of apparent heat source Q_1 obtained as a residual of the budget calculation in eq. (4) is shown in Fig. 9. There exists a large apparent heat source throughout the whole troposphere, with a primary maximum at 400 mb and a secondary peak at 715 mb, and a slight minimum near 600 mb. The large value of Q_1 in the low levels (peak at 715 mb) results mainly from large positive values of vertical

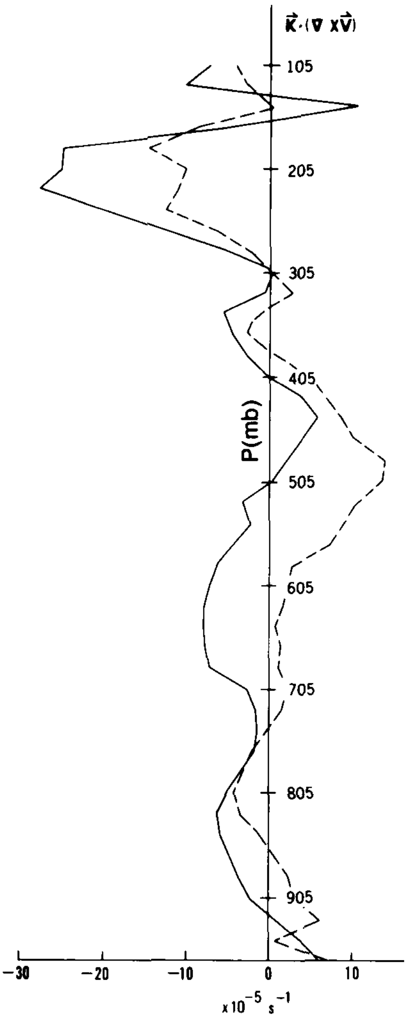

Fig. 7. Relative vorticity profiles for 1630 CST (——) and 1800 CST (– – – –).

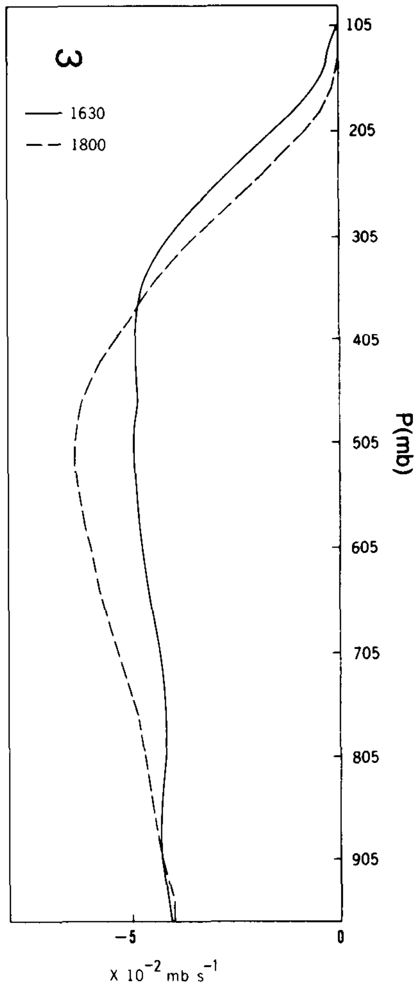

Fig. 8. Adjusted vertical *p*-velocity for 1630 CST (———) and 1800 CST (– – – –).

advection. On the other hand, the upper-level large value of Q_1 is due mainly to large positive values of horizontal advection. The local change term in the budget equation of Q_1 is negligible compared to the advection terms throughout the whole troposphere.

The time-averaged vertical profile of the apparent moisture sink Q_2 shown in Fig. 9 is obtained from the budget model in eq. (5). Although there are large fluctuations in both the Q_1 and Q_2 profiles, the vertical profiles are different. This was used as a measure of the activity of cumulus convection (Wada, 1969; Nitta, 1972). The averaged Q_2 has its principal maximum at 655 mb and a secondary maximum at 495 mb. The large value of Q_2 near the surface results from a large positive value of vertical advection. This large apparent moisture sink implies the existence of strong compensating subsidence in the subcloud layer induced by cumulus clouds. A moisture source ($Q_2 < 0$) appeared in the middle layer near 595 mb, suggesting evaporation at the top of small clouds.

In analogy to an apparent heat source and an apparent moisture sink, we evaluate the apparent

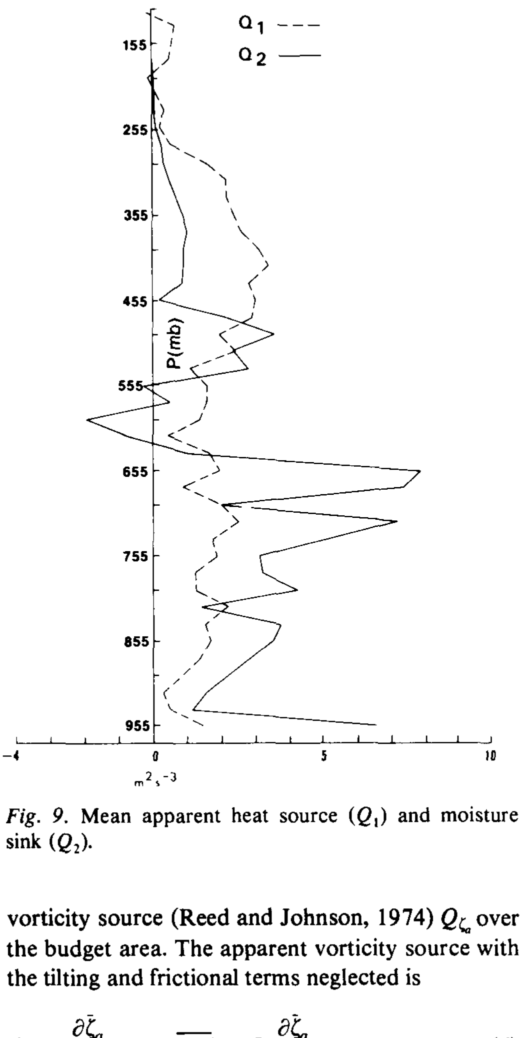

Fig. 9. Mean apparent heat source (Q_1) and moisture sink (Q_2).

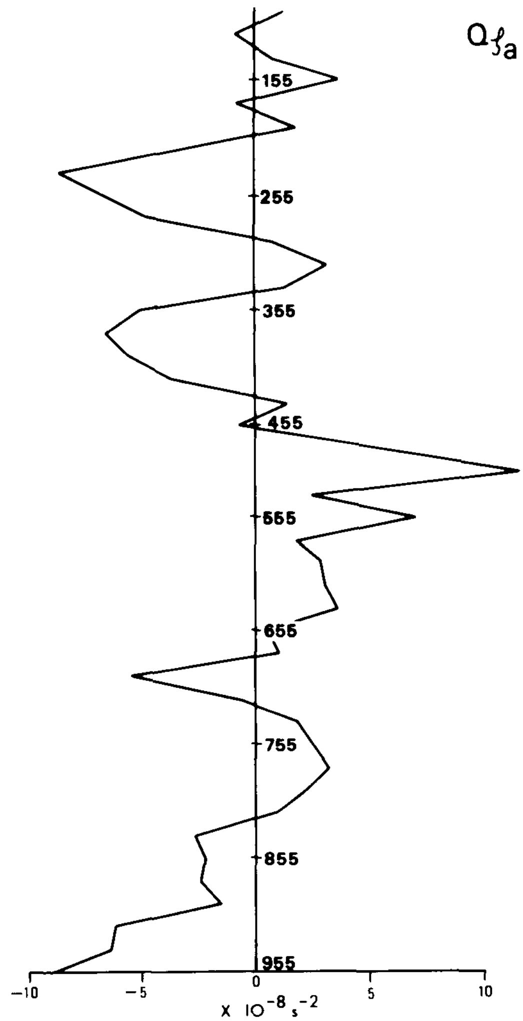

Fig. 10. Mean apparent vorticity source.

vorticity source (Reed and Johnson, 1974) Q_{ζ_a} over the budget area. The apparent vorticity source with the tilting and frictional terms neglected is

$$Q_{\zeta_a} = \frac{\partial \bar{\zeta}_a}{\partial t} + \nabla \cdot (\overline{\zeta_a \mathbf{v}}) + \bar{\omega} \frac{\partial \bar{\zeta}_a}{\partial p} \tag{6}$$

where $\bar{\zeta}_a = \bar{\zeta} + f$ is an absolute vorticity, $\bar{\zeta} = \partial \bar{v}/\partial x - \partial \bar{u}/\partial y$, a relative vorticity and f is the coriolis parameter. Overbars denote area average.

The evaluation of Q_{ζ_a} in eq. (6) actually includes the residual, the tilting and the frictional effects. But the frictional effect is confined to very shallow layers near the surface. If the tilting effect on Q_{ζ_a} is small, as is usually assumed, the increased value of Q_{ζ_a} in eq. (6) probably indicates increases in near-environment vorticity by cumulus convection. Fig. 10 shows the vertical profile of the apparent vorticity source in the budget area. An apparent sink exists in the lower troposphere and the upper troposphere, and an apparent source exists in the mid troposphere for the near-environmental vorticity. In the lower troposphere the individual change of absolute vorticity ($d\bar{\zeta}_a/dt$) following the mean motion is the dominant term in the budget, especially the vertical advection term $[\bar{\omega}(\partial \bar{\zeta}_a/\partial p)]$, but in the upper troposphere the vorticity production term (divergence term, $\bar{\zeta}_a \overline{\nabla \cdot \mathbf{v}}$) is the dominant term in the budget. The anticyclonic relative vorticity in the upper troposphere is larger than the earth's vorticity, and the flow is divergent (i.e. $f + \bar{\zeta} < 0$ and $\overline{\nabla \cdot \mathbf{v}} > 0$); therefore, a negative residual (apparent vorticity sink) occurs in the upper divergent layer. The low-level apparent vorticity sink and the mid-level source are presumably to be attributed to vertical transport by cumulus convection, namely, the removal of low-level cyclonic vorticity-rich air to mid-troposphere layers by convective motions. However, the mechanism of the upper-level sink is not quite clear. In order to understand the mechanism involved, the vorticity budget should be examined in detail, considering especially dynamic and thermodynamic coupling in the model. For example, vorticity and its generation may be influenced by large-scale divergence. Moisture convergence or divergence may result in changes in the thermodynamic field and the cloud mass flux.

5. A simple diagnostic cloud model

The gross effects of clouds on the near-environment mass, moisture and heat fields can be examined from the budget results in the previous section. However, the detailed interactions between the clouds and the environment cannot be explained without a diagnostic cloud model. Therefore, we utilize a simple area averaged cloud model derived from the conservation laws.

The Eulerian derivative of any conservation quantity λ can be written

$$\frac{d\lambda}{dt} = \frac{\partial \lambda}{\partial t} + \mathbf{v}\cdot\nabla\lambda + \omega\frac{\partial\lambda}{\partial p} = 0 \tag{7}$$

Integrating eq. (7) over a hypothesized horizontal area $A = A(p, t)$ and applying the Leibnitz rule for variable boundaries yields (see Fraedrich, 1973)

$$\frac{\partial}{\partial t}(\lambda_a A) - \lambda_B\frac{\partial A}{\partial t} + \frac{\partial}{\partial p}(\omega_a\lambda_a) - \lambda_B\frac{\partial \omega_a}{\partial p} = 0 \tag{8}$$

We assume that the vertical mass transports at the lateral boundaries vanish, and

$\lambda_a A = \int_A \lambda dA$

$\omega_a = \int_A \omega dA$ an area weighted vertical p-velocity

and λ_B is the value at the boundary of the area A, and depends upon the sign of $\partial A/\partial t$ and $\partial\omega_a/\partial p$.

The area-averaged eq. (8) is applied to the cloud area to give

$$\frac{\partial}{\partial t}(\lambda_c\sigma) - \lambda_B\frac{\partial\sigma}{\partial t} + \frac{\partial}{\partial p}(\omega_c\lambda_c) - \lambda_B\frac{\partial\omega_c}{\partial p} = 0 \tag{9}$$

where σ is the fraction of the horizontal area occupied by the active cloud and the boundary values λ_B are defined by

$$\lambda_B = \begin{cases} \lambda_e, & \text{for } \dfrac{\partial\sigma}{\partial t} + \dfrac{\partial\omega_c}{\partial p} > 0 \ \text{(entrainment layer)} \\ \lambda_c, & \text{for } \dfrac{\partial\sigma}{\partial t} + \dfrac{\partial\omega_c}{\partial p} < 0 \ \text{(outflow layer)} \end{cases}$$

From now on we consider the steady-state (i.e., $\partial()/\partial t \equiv 0$) cloud model considered by Yanai et al. (1973), Nitta (1977), etc. This assumption implies that the activity of clouds is statistically in equilibrium with their environment. Even though individual clouds evolve in their own life cycles, clouds over a time scale equal to the life cycle of the storm maintain a heat and moisture balance with the environment.

Neglecting the storage terms, eq. (9) reduces to

$$\frac{\partial\lambda_c}{\partial p} = \frac{1}{\omega_c}\frac{\partial\omega_c}{\partial p}(\lambda_B - \lambda_c) \tag{10}$$

In this case the entrainment layer is defined by $\partial\omega_c/\partial p > 0$ and the outflow layer by $\partial\omega_c/\partial p < 0$. If we define the entrainment rate $\varepsilon = (1/\omega_c)(\partial\omega_c/\partial p)$ and assume that it is constant with height, the vertical distribution of the mass flux within the clouds is given by:

$$\omega_c = \omega_{c0}\exp[\varepsilon(p - p_0)] \tag{11}$$

where ω_{c0} is the vertical p-velocity at the cloud base $p = p_0$.

Since the total energy (moist static energy) is approximately conserved for both dry and moist adiabatic processes (Yanai et al., 1973) for inviscid and steady motion, we substitute λ by $h = c_pT + gz + Lq$, where g is gravity and z height, and λ_B by λ_e in eq. (10) leads to an equation for the moist static energy in the entrainment layer:

$$\frac{\partial h_c}{\partial p} = \varepsilon(h_e - h_c) \tag{12}$$

In the detrainment layer, $\lambda_B = \lambda_c$. From eq. (10) the moist static energy is given by

$$\omega_c\frac{\partial h_c}{\partial p} = 0 \tag{13}$$

The vertical distribution of cloud mass flux (or cloud vertical velocity) in the detrainment layer may be used in an analogous relation to that in the entrainment layer given in eq. (11), but with a different ε, or it can be estimated by using an apparent moist static energy with cloud parameterization. However, in order to close the cloud mass flux profile in the detrainment layer and for simplicity, we have assumed a profile that satisfies the relationship as follows:

$$\omega_c = k_1 \, \omega_e \tag{14}$$

where the proportionality k_1 is determined by the upper boundary values of the entrainment layer. All the other thermodynamic cloud variables can then be evaluated from eq. (9) applied on a steady-state. The net changes of static energy S and latent heat Lq depend on the condensation rate C and the evaporation rate E:

$$\frac{\partial}{\partial p}(\omega_c q_c) - q_B \frac{\partial \omega_c}{\partial p} + (C - E) = 0 \tag{15}$$

and

$$\frac{\partial}{\partial p}(\omega_c S_c) - S_B \frac{\partial \omega_c}{\partial p} - L(C - E) = 0 \tag{16}$$

where

$$q_B, S_B = \begin{cases} q_e, S_e & \text{in the entrainment layer} \\ q_c, S_c & \text{in the detrainment layer} \end{cases}$$

From the assumptions that the air is saturated in the clouds, and the effect of a pressure difference between the cloud and the environment on q_s, where subscript s denotes the saturation value, can be neglected (see Arakawa and Schubert, 1974), then

$$q_c = q_s + \frac{\gamma}{L} \frac{1}{\gamma + 1}(h_c - h_s) \tag{17}$$

and

$$S_c - S_e = \frac{1}{\gamma + 1}(h_c - h_s) \tag{18}$$

where $\gamma = (L/C_p)(\partial q_s/\partial_{\bar{T}})_p$, and $h_s = S_e + Lq_s$ is the saturation value of moist static energy of the environment, and bar quantities are the average values of the environment.

Using the Clausius–Clapeyron equation and neglecting the effect of temperature on the latent heat of condensation, which is considered to be small (Hess, 1959), at each pressure level we get

$$\lambda \cong \frac{0.622 e_{s0} L^2}{R_v \bar{T}^2 p C_p} \exp\left[\frac{L}{R_v}\left(\frac{1}{273.16} - \frac{1}{\bar{T}}\right)\right] \tag{19}$$

where R_v is the gas constant for water vapor and e_{s0} is the saturation vapor pressure at $T = 273.16$ K.

5.1. *Boundary conditions*

Several boundary conditions at the cloud base p_0 are needed to close the system. Such conditions are described by Yanai et al. (1973), Arakawa and Schubert (1974) and others. These conditions are mainly determined by a suitable subcloud layer model. However, the coupling between the cloud layer and subcloud layer is not yet clearly understood for mid-latitude severe thunderstorms. In this study we will assign proper values according to basic governing physics and observed data.

The cloud base p_0 can be determined by the level where a parcel that originated at the surface becomes buoyant, that is, h_e (surface) $= h_s(p_0)$ if the parcel were pseudo-adiabatically brought to saturation. The cloud top p_t can also be defined by the thermodynamic condition $h_c(p_t) = h_s(p_t) \simeq h_e(p_t)$. The buoyant cloud parcel loses its buoyancy as h_c approaches its environment value h_e. Still unknown cloud parameters such as ε (entrainment rate), ω_{c0} (vertical velocity at the base of cloud) are needed to resolve the cloud properties. The entrainment rate ε varies widely, study by study. For example, in small (1–2 km) tropical cumuli (Stommel, 1947) the entrainment rate was assumed to be 1.0 km^{-1}, in continental cumulus congestus (Sloss, 1967) $\varepsilon \simeq$ 0.1–0.4 km^{-1}, and in growing cumulus cloud (Byers and Braham, 1949) ε about 0.2 km^{-1}. We will consider two different values of ε, 10^{-3} mb^{-1} and 2×10^{-3} mb^{-1}, so that we may examine the sensitivity of the other derived variables on ε, ω_{c0} at the cloud base is unknown *a priori*. Since the environmental mass flux is directly related to cloud mass flux at the cloud base, we assumed ω_{c0} to be the observed environmental p-velocity at p_0.

6. Application of the cloud model to the 20 May storm

Fig. 11 shows the profiles of the vertical p-velocities in the cloud for two different entrainment rates, $\varepsilon = -0.001$ mb^{-1} and -0.002 mb^{-1}. For both entrainment rates the lower boundary condition was used as the value of the adjusted environmental vertical velocity as mentioned in the

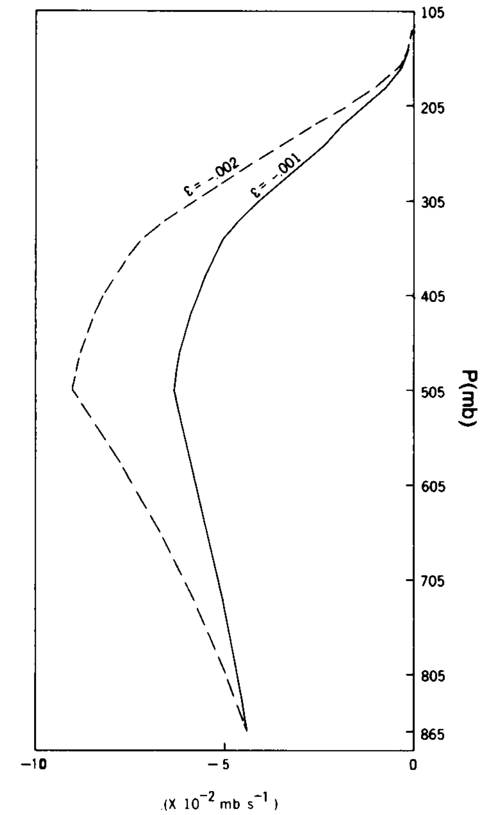

Fig. 11. Vertical profiles of cloud p-velocity for assumed two different values of ε.

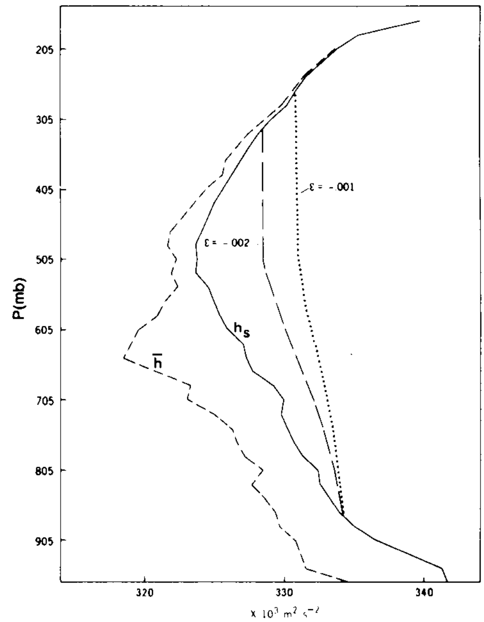

Fig. 12. Moist static energy in the near environment $\bar{h}$, saturation moist static energy h_s and cloud moist static energy for $\varepsilon = -0.001$ mg^{-1} (....) and $\varepsilon = -0.002$ mb^{-1} (– – – –).

previous section, and the top of entrainment layer was assumed as the level where the sounding p-velocity is maximum, $p = 505$ mb. The upward vertical velocity in clouds is larger than the required time- and space-averaged horizontal convergence (or the sounding p-velocity) mainly due to active convection in clouds.

Fig. 12 shows the vertical distributions of moist static energy for different values of the entrainment rates compared with that in the near environment $\bar{h}$ and its saturation value h_s. The moist static energy in the clouds evaluated using eq. (12) decreases with height, due to dilution through the entrainment from the environment. The larger the entrainment rate the smaller the moist static energy in the clouds h_c. Above 505 mb the cloud moist static energy h_c is constant with height because we assumed $\partial h_c/\partial p = 0$ in the outflow layer. The thickness of the cloud decreases as the entrainment rate ε increases. The top of the cloud, which is given by the condition $h_s(p_t) = h_c(p_t)$, is at 265 mb for $\varepsilon = -0.001$ mb^{-1} and at 325 mb for $\varepsilon = -0.002$ mb^{-1}.

The excess moist static energy above the saturation value in the near-environment is presented in Fig. 13a. The excess reaches its maximum (7.5×10^3 m^2 s^{-2} for $\varepsilon = -0.001$ and 5×10^3 m^2 s^{-2} for $\varepsilon = -0.002$) near 525 mb.

Using the budget area sounding data, the function γ at each pressure level is evaluated from eq. (19). The result is quite similar to that of Jordan (1958) obtained from mean soundings in the West Indies during the hurricane season. This function was used to calculate excess values of static energy (Fig. 13b), temperature (Fig. 13c) and mixing ratio (Fig. 14), from eqs. (17) and (18) for different values of the entrainment rate. The excess static energy increases from the cloud bottom up to 485 mb, where the maximum values are 4.7×10^3 m^2 s^{-2} for $\varepsilon = -0.001$ mb^{-1}, and 3.2×10^3 m^2 s^{-1} for $\varepsilon = -0.002$ mb^{-1}. A similar pattern for excess temperature is shown in Fig. 13c, since the excess temperature is estimated by $T_c - T_e = C_p^{-1} (S_c - S_e)$.

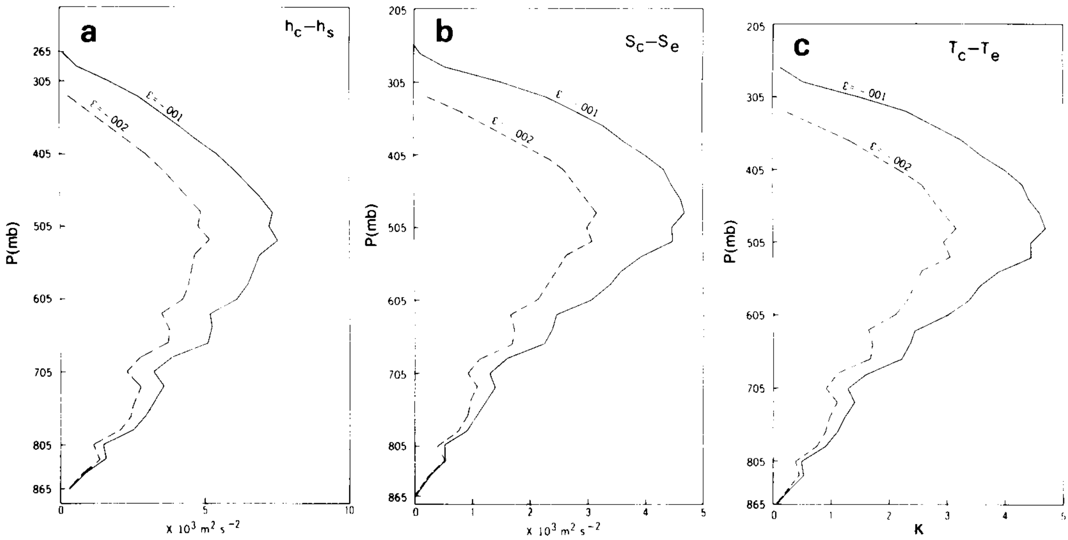

Fig. 13. Vertical distributions of excess (a) moist static energy, (b) static energy and (c) temperature (K) for different values of entrainment rate.

The maximum excess temperatures are 4.7°C for $\varepsilon = -0.001$ mb^{-1} and 3.2 °C for $\varepsilon = -0.002$ mb^{-1} at 485 mb. These values are slightly larger than those of Malkus (1958) for shallow trade cumuli in the Caribbean, where the excess temperature of shallow cumuli is about 2 °C. The maximum magnitudes of excess moisture are 5.2 g/kg for $\varepsilon = -0.001$ mb^{-1} and 4.9 g/kg for $\varepsilon = -0.002$ mb^{-1} and occur at 665 mb. The change of entrainment rate does not significantly affect the size of the excess mixing ratio (Fig. 14).

Cloud models are often justified by comparing the quantities obtained from the model and those observed. For this purpose, we estimated the condensation rate per unit area. Because measurements of the total mean liquid water content of the atmosphere were not available and the effects of downdraft (or evaporation rate) were neglected in this model, the net condensation rate in the cloud would equal the precipitation rate only provided that storage of liquid water in the cloud is assumed negligible.

The condensation rate can be estimated from eq. (15), neglecting the evaporation rate (i.e., $E = 0$). In the entrainment layer, $q_B = q_e$, thus

$$C = (q_e - q_c)\frac{\partial \omega_c}{\partial p} - \omega_c \frac{\partial q_c}{\partial p}$$

and in the outflow layer $q_B = q_c$, therefore

$$C = -\,\omega_c \frac{\partial q_c}{\partial p}$$

The vertical profiles of the condensation rate are shown in Fig. 15 for the two values of the entrainment rate. The maximum condensation rates are $14{\cdot}18 \times 10^{-4}$ g kg^{-1} s^{-1} at 495 mb for $\varepsilon = -0.001$ mb^{-1} and 19.50×10^{-4} g kg^{-1} s^{-1} for $\varepsilon = -0.002$ mb^{-1}. The total condensation rate C_t per unit column of cloud is estimated by

$$C_t = \frac{1}{g}\int_{p_0}^{p_t}\left[(q_e - q_c)\frac{\partial \omega_c}{\partial p} - \omega_c\frac{\partial q_c}{\partial p}\right] dp,$$

$$\text{for } \frac{\partial \omega_c}{\partial p} > 0$$

and

$$C_t = \frac{1}{g}\int_{p_0}^{p_t} -\,\omega_c \frac{\partial q_c}{\partial p}\, dp, \quad \text{for } \frac{\partial \omega_c}{\partial p} < 0$$

The evaluated total condensation rates per unit area through the vertical column of the cloud are $C_t = 23.0$ kg m^{-2} h^{-1} for $\varepsilon = -0.001$ mb^{-1} and 26.1 kg m^{-2} h^{-1} for $\varepsilon = -0.002$ mb^{-1}. These values are in good agreement with observed average rainfall of 26.8 kg m^{-2} h^{-1} (see Fig. 5) in the NSSL

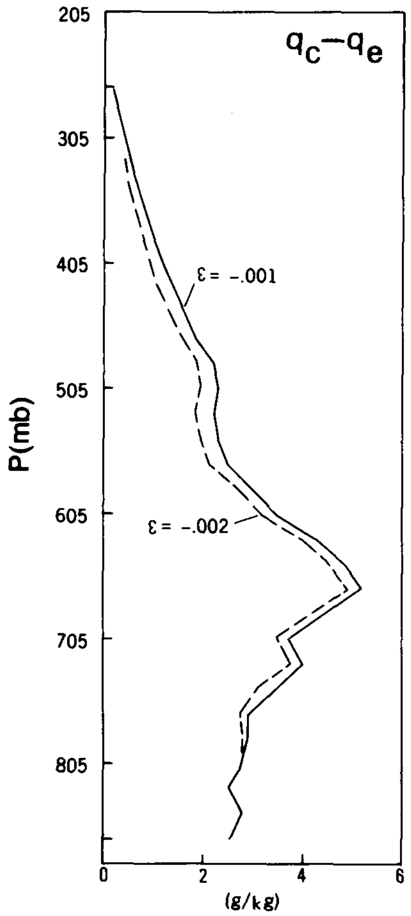

Fig. 14. Vertical distribution of excess mixing ratio for different values of entrainment rate.

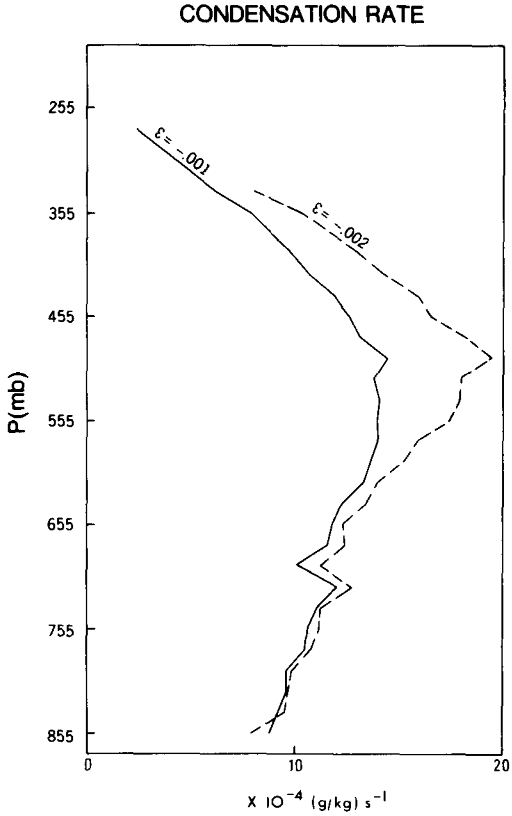

Fig. 15. Vertical profiles of condensation rate for different values of entrainment rate.

meso-network from 1630 CST to 1800 CST, taking into account the accuracy of the field observations and the assumptions made.

The total moisture convergence per unit area within the cloud column may be estimated by

$$-\frac{1}{g}\int_{p_0}^{p_t} \omega_c \frac{\partial q_c}{\partial p}\, dp$$

which is 25.3 kg m^{-2} h^{-1} for $\varepsilon = -0{\cdot}001$ mb^{-1}; on the other hand, the contribution of lateral mixing to the condensation rate is 2.3 kg m^{-2} h^{-1}. This shows that only 9% of the vapor convergence goes to the lateral mixing processes, the rest falling out as precipitation. For $\varepsilon = -0.002$ mb^{-1}, the total convergence of water vapor within the cloud column per unit area is about 31.3 kg m^{-2} h^{-1}, and about 16.7% (about 5.2 kg m^{-2} h^{-1}) of the total water vapor convergence is dispersed in lateral mixing.

The production of kinetic energy by cumulus activities per unit area of a column of the cloud can be estimated by

$$E = -\frac{R}{g}\int_{p_0}^{p_t} \overline{\omega' T'}\, dlnp$$

where R is the gas constant. Following Yanai et al. (1973) this can be written

$$E = -\frac{R}{c_p g}\int_{p_0}^{p_t} \omega_c (S_c - S_e)\, dlnp$$

The estimated values in this case are $E = 1{\cdot}80 \times 10^3$ kJ m^{-2} h^{-1} and 1.44×10^3 kJ m^{-2} h^{-1} for the entrainment rate $\varepsilon = -0.001$ mb^{-1} and -0.002 mb^{-1}, respectively. The rate of release of latent heat of condensation (i.e. LC_t) in the column of the cloud per unit area is 6.32×10^4 kJ m^{-2} h^{-1} and 6.52×10^4 kJ m^{-2} h^{-1} for $\varepsilon = -0.001$ mb^{-1} and -0.002 mb^{-1}, respectively. The ratio of the production of kinetic energy E to the release of latent heat due to condensation in the cloud column per unit area is this case 2.85% and 2.21% for $\varepsilon = -0.01$ mb^{-1} and -0.002 mb^{-1}, respectively.

7. Summary

The vertical distributions of the apparent heat source and the moisture sink in the storm complex are found similar to those found in tropical regions (Nitta, 1977). However, the apparent vorticity source in this study appear different from those observed in tropical regions (Reed and Johnson, 1974). We found a large apparent vorticity sink in the upper divergent layer. This upper-level sink cannot be explained by the vertical transport of vorticity due to cumulus-convection mechanism alone; other mechanisms including thermodynamic effects are likely to be important.

Simple parameterization of deep convection involving mass transport and lateral mixing (Kuo, 1965) can be examined with the assumed entrainment rates and the conservative quantities. Clearly, the dominant term is vertical mass transport. The total contribution of lateral mixing due to cumulus activities represents 9% for $\varepsilon = -0.001$ mb^{-1} and 16.7% for $\varepsilon = -0.002$ mb^{-1} of the total moisture convergence. With these relatively small entrainment rates the model-estimated condensation rate is comparable with the observed precipitation rate, but with relatively large entrainment rates ($\varepsilon > -0.004$ mb^{-1}) the cloud is too shallow to obtain realistic results. The reasonable entrainment rate for this case is about -0.002 mb^{-1}.

The present simple cloud model may be improved by including the proper parameterizations of the environmental vertical wind shear (Newton, 1966) usually observed in the thunderstorm environment, of the storage effects (Betts, 1973; McNab and Betts, 1978), and of the subcloud layer modeling. These will be considered in future case studies.

8. Acknowledgements

The authors wish to thank Professor David H. Miller for editorial comments during the preparation of this manuscript. The surface and upper air data used in this research were furnished by the National Severe Storms Laboratory, Oklahoma, and the satellite data obtained from the Space Science and Engineering Center, University of Wisconsin-Madison. Donald Temple drafted the diagrams.

The research reported in this paper was supported by the National Science Foundation under Grant No. ATM 77-24842, and the Graduate School, University of Wisconsin-Milwaukee.

REFERENCES

Arakawa, A. and Schubert, W. H. 1974. Interaction of a cumulus cloud ensemble with the large-scale environment, Part I. *J. Atmos. Sci. 31*, 674–701.

Betts, A. K. 1973. A composite mesoscale cumulus budget. *J. Atmos. Sci. 30*, 597–610.

Byers, H. R. and Braham, R. R. 1949. The thunderstorms. Washington, Govert. Print. Off., 287 pp.

Fankhauser, J. C. 1969. Convective processes resolved by a mesoscale rawinsonde network. *J. Appl. Meteor. 8*, 778–798.

Fankhauser, J. C. 1974. The derivation of consistent fields of wind and geopotential height from mesoscale rawinsonde data. *J. Appl. Meteor. 6*, 637–646.

Fraedrich, K. 1973. On the parameterization of cumulus convection by lateral mixing and compensating subsidence. Part I. *J. Atmos. Sci. 30*, 408–413.

Hess, S. L. 1959. Introduction to theoretical meteorology. Holt, Rinehart and Winston, New York, 362 pp.

Jordan, C. L. 1958. Mean soundings for the West Indies area. *J. Meteor. 15*, 91–97.

Kuo, H. L. 1965. On formation and intensification of tropical cyclones through latent heat released by cumulus convection. *J. Atmos. Sci. 22*, 40–63.

Malkus, J. S. 1952. Some results of a trade-cumulus cloud investigation. *J. Meteor. 11*, 220–237.

McNab, A. L. and Betts, A. K. 1978. A mesoscale budget study of cumulus convection. *Mon. Wea. Rev. 106*, 1317–1331.

Newton, C. W. 1966. Circulations in large sheared comulonimbus. *Tellus 18*, 699–712.

Newton, C. W. and Katz, S. 1958. Movement of large convective rainstorms in relation to winds aloft. *Bull. Amer. Meteor. Soc. 39*, 129–136.

Nitta, T. 1972. Energy budgets of wave disturbances over the Marshall Islands during the years of 1956 and 1958. *J. Meteor. Soc. Japan 50*, 71–84.

Nitta, T. 1977. Response of cumulus updraft and downdraft to GATE A/B scale motion systems. *J. Atmos. Sci. 34*, 1163–1186.

O'Brien, J. J. 1970. Alternative solutions to the classical vertical velocity problem. *J. Appl. Meteor. 9*, 197–203.

Ogura, Y. and Cho, H.-R. 1973. Diagnositic determination of cumulus cloud populations from large-scale variables. *J. Atmos. Sci. 30*, 1276–1286.

Reed, R. J. and Johnson, R. H. 1974. The vorticity budget of synoptic-scale wave disturbances in the tropical western Pacific. *J. Atmos. Sci. 31*, 1784–1790.

Sloss, P. W. 1967. An empirical examination of cumulus entrainment. *J. Appl. Meteor.* **5**, 878–881.

Stommel, H. 1947. Entrainment of air into a cumulus cloud. *J. Meteor. 4*, 91–94.

Wada, M. 1969. Concerning the mechanism of the decaying of typhoon. *J. Meteor. Soc. Japan 47*, 335–351.

Yanai, M., Esbensen, S. and Chu, J. 1973. Determination of average bulk properties of tropical cloud clusters from large-scale heat and moisture budgets. *J. Atmos. Sci. 30*, 611–627.

ПРИМЕНЕНИЕ ПРОСТОЙ ДИАГНОСТИЧЕСКОЙ МОДЕЛИ ОБЛАКА К УРАГАНУ 20 МАЯ 1977 Г. НАД МЕЗОМАСШТАБНОЙ СЕТЬЮ В ОКЛАХОМЕ

Для урагана 20 мая 1977г. с использованием данных мезомасштабной сети наблюдений Национальной лаборатории ураганов с помощью кинематических соотношений были вычислены средние мезомаштабные величины атмосферы, такие, как масса, влажность и завихренность, которые приводят к сильному дождю. К данным по урагану применяется простая равновесная модель облака, полученная на основе законов сохранения. Осадки, оцененные при помощи скорости конденсации в модели облака, довольно хорошо согласуются с таковыми, наблюденными на поверхности земли. Полная энергия системы урагана поддерживается в основном высвобождением скрытой теплоты.